

https://dspace.org/

Spatial and Temporal Patterns of Rainfall Erosivity in Southern Africa in Extreme Wet and Dry Years

Jasper Knight; M Abd Elbasit

MDPI AG
https://hdl.handle.net/10539/42517
WOS

Downloaded from a DSpace repository. https://dspace.org/

atmosphere

MDPI

Article

Spatial and Temporal Patterns of Rainfall Erosivity in Southern Africa in Extreme Wet and Dry Years

Jasper Knight [1,*] and Mohamed A. M. Abd Elbasit [2]

[1] School of Geography, Archaeology and Environmental Studies, University of the Witwatersrand, Johannesburg 2050, South Africa
[2] Faculty of Natural and Applied Sciences, Sol Plaatje University, Kimberley 8301, South Africa; mohamed.ahmed@spu.ac.za
* Correspondence: jasper.knight@wits.ac.za

Abstract: Soil erosivity is a key indicator of the effectiveness of precipitation acting on the land's surface and is mainly controlled by event-scale and seasonal weather and climatic factors but is also influenced by the nature of the land's surface, including relief and vegetation cover. The aim of this study is to examine spatial and temporal variations in soil erosivity across southern Africa using rainfall data for the period 2000–2023 and a gridded raster spatial modelling approach. The two wettest and driest years in the record (±>1.5 standard deviation of rainfall values) were identified, which were 2000 and 2006, and 2003 and 2019, respectively. Monthly rainfall values in these extreme wet/dry years were then analyzed for four rainfall regions (arid, semiarid, subhumid, humid), identified according to their annual rainfall totals. These data were then used to calculate Precipitation Concentration Index (PCI) values as an expression of rainfall seasonality, and the modified Fournier index (MFI) was used to quantify rainfall erosivity. The results show that there are significant differences in erosivity between the different climate regions based on rainfall seasonality and also their distinctive environmental settings. In turn, these reflect the synoptic climatic conditions in these regions, their different precipitation sources, and rainfall totals. The results of this study show that calculated MFI values at the national scale, which is the approach taken in most previous studies, cannot effectively describe or account for erosivity values that characterize different climatic regions at the sub-national scale. Furthermore, the mismatch between PCI and MFI spatial patterns across the region highlights that, under semiarid, and highly seasonal rainfall regimes, episodic rainfall events interspersed with periods of dryness result in significant variability in erosivity values that are unaccounted for by rainfall totals or seasonality alone. In these environments, flash floods and wind erosion result in regional-scale soil erosion and land degradation, but these processes and outcomes are not clear when considering MFI values alone. Fully evaluating spatial and temporal patterns of erosivity in their climatic and environmental contexts, as developed in this study, has implications for sediment and carbon exports, as well as identifying the major regions in which land degradation is an environmental and agricultural issue.

Keywords: erosivity; Fournier index; rainfall climatology; seasonality; soil erosion modelling; South Africa

check for updates

Citation: Knight, J.; Abd Elbasit, M.A.M. Spatial and Temporal Patterns of Rainfall Erosivity in Southern Africa in Extreme Wet and Dry Years. *Atmosphere* **2024**, *15*, 1283. https://doi.org/10.3390/atmos15111283

Academic Editors: Yang Yu, Lei Wang and Cun Chang

Received: 5 September 2024
Revised: 12 October 2024
Accepted: 25 October 2024
Published: 26 October 2024

Copyright: © 2024 by the authors. Licensee MDPI, Basel, Switzerland. This article is an open access article distributed under the terms and conditions of the Creative Commons Attribution (CC BY) license (https://creativecommons.org/licenses/by/4.0/).

1. Introduction

1.1. Rainfall Climatology and Applications to Erosivity in Africa

In southern Africa, several recent studies have identified and analyzed extreme precipitation events that have the potential to lead to anomalously wet or dry land surface conditions and, typically, floods and droughts, respectively [1–3]. These precipitation extremes arise as a result of changes in long-term synoptic atmospheric circulation patterns, changes in naturally occurring climate cycles such as the El Niño–Southern Oscillation (ENSO) and the Indian Ocean Dipole (IOD) [4,5], and the occurrence of high-magnitude

events such as tropical cyclones [6,7]. Studies have also examined rainfall patterns over different spatial and temporal scales, from a continental scale [7] to that of individual river basins [6,8], and from mean annual [9] to seasonal [10–12] and daily time scales [13,14]. Although many of these studies have been concerned with the implications of changing rainfall patterns for rivers and flood risk, agricultural production, and community health, amongst others [3,8,15], relationships to spatial and temporal rainfall erosivity have not been a major focus [16,17]. This is despite many studies examining erosivity at a regional to continental scale in Africa, where rainfall patterns (rather than local environmental conditions) are the major controls on calculated erosivity values [18–21].

Rainfall erosivity is an important proxy for the likelihood of land surface erosion to take place and is derived from the interaction of rainfall properties (e.g., 30 min erosivity intensity (EI_{30}), rainfall total over 3 h to seasonal timescales) with the land surface [22–25]. Rain gauge records have been brought together in the Global Rainfall Erosivity Database [20,21], and this database can be used to map spatial patterns of erosivity across regional scales. In addition, erosivity is also closely related to spatial patterns of land surface properties such as geology, relief (terrane form), slope, soil type, vegetation cover, and land use. Several studies have examined the interplay between these properties in terms of their contribution to net erosivity in different locations and under different rainfall regimes [17,26].

As a result of rainfall variability across different land surfaces, several studies have been concerned with evaluating spatial and temporal trends in rainfall erosivity in different locations in Africa. For example, Fenta et al. [27] showed that the highly variable topography of East Africa results in spatially variable patterns of rainfall, where low-lying coasts are affected by frontal and cyclonic systems and highland areas are affected by orographic rainfall. These different weather systems have different patterns of rainfall (timing, length, intensity). The outcome is highly variable mean erosivity values across the region, corresponding to the synoptic weather systems present, with accompanying high seasonal variability in both erosivity and parameters derived from rainfall data such as the Precipitation Concentration Index (PCI). In northern Algeria, despite average erosivity values declining over time between 1970 and 2008 as a result of an overall aridity trend, land surface erosion and the siltation of dams have actually increased, likely as a result of human-induced land use change [28,29]. This highlights how rainfall forcing itself is not the only factor contributing to erosion patterns, especially in regions that have high spatial and temporal variability in rainfall or that are extensively modified by agriculture.

1.2. Approaches to Evaluating Rainfall Erosivity

A common approach to evaluating erosivity is through the application of the Universal Soil Loss Equation (USLE) and its derivations [30,31]. This has been widely employed across Africa to consider soil erosion risk, especially in high-relief mountain areas [19,32]. Erosivity is expressed through the *R*-factor in the USLE, and this is given in units of MJ mm ha^{-1} h^{-1} yr^{-1} [18,33]. The use of *R*-factor values enables the results of different studies to be compared. At a global scale and derived from a large database, mean *R*-factor values are calculated as 2190, but these are significantly different between the northern (1545) and southern hemispheres (4545) and between the summer (41–47% of total annual erosivity) and winter seasons (8–10% of total annual erosivity) [21]. However, only 4% of rainfall erosivity stations in this database are located in Africa, and thus, the applicability of these calculated values to this area is not clear. Average *R*-factor annual values in Algeria range from 107 to 871 [28]. In East Africa, annual values range from 1895 to 3246 [27]. Annual values from Ibadan and Port Harcourt in Nigeria are 213 and 361, respectively; however, based on the erosivity resulting from event-scale rainfall only at these locations (EI_{30} and EI_{15}), the extrapolated annual values are 9742 and 15,752, respectively, indicating the important role of event-scale rainfall in soil erosion [24]. These different examples from Africa show that *R*-values are highly variable, irrespective of the spatial and temporal scales of analysis.

The modified Fournier index (MFI) is also commonly used to calculate rainfall erosivity based on long-term datasets of monthly rainfall data for a region [34]. The advantage of this approach is that it is based on aggregated monthly data only, and such data are commonly available even from low-resolution or poorly resourced weather stations, which makes it ideal for many locations in Africa. For example, in Sudan, MFI values are significantly low throughout the period 1941–2007, but significant high-value peaks exist related to episodes of much higher rainfall [35]. In Algeria, MFI values are positively correlated with El Niño state and, thus, the cyclicity of rainfall patterns [29]. In Ethiopia, spatial gradients in MFI values are present, related to altitude, but there is a generally decreasing trend for all regions for the period 2000–10 that reflects decreased rainfall [36]. However, the observation of increased soil erosion rates despite decreased erosivity implies that factors such as overgrazing and land use change are the main drivers. In Rwanda, the opposite is found where MFI values show an increasing trend over time (1960s–1990s) [37].

More recently, regional-scale rainfall patterns can be derived and have been analyzed from remotely sensed datasets such as Tropical Rainfall Measurement Mission (TRMM) products [38]. In West Africa, comparison with rainfall data derived from other datasets shows that TRMM data perform well and with lower errors over monthly/seasonal time scales and over large aggregated (2.5° × 2.5°) grid cell scales [39]. This has been used in a spatial sense to model rainfall erosivity across regions, such as many areas of Africa, where there is an absence of field-based rain gauge data [33]. Analysis of the TRMM Multi-satellite Precipitation Analysis (TMPA) dataset shows that, although this dataset has spatial advantages, it is insufficient to accurately model erosivity values. Vrieling et al. [18] found that MFI has a higher correlation coefficient (r = 0.84) than the 3 h TMPA data product (r = 0.71). Thus, the use of MFI based on monthly rainfall data is recommended, and for this reason, this is focused on in this study.

1.3. Limitations of Previous Work and This Study's Aim

Although there are studies of rainfall erosivity in some areas of Africa, there are few from southern Africa [16,17,40], which is surprising given its seasonal and highly variable rainfall regime and the relationships of rainfall to agricultural production and climate hazards. Although spatial patterns of erosivity are identified on maps presented in these previous studies, these patterns are not linked to the different rainfall regimes that are found across South Africa [41]. Likewise, there is no consideration of the temporal patterns of erosivity caused by rainfall seasonality. This research gap is particularly important given that changes in seasonal rainfall patterns (season timing, duration, total rainfall) are already being observed [11,42] and that event-scale rainfall is also increasing [14].

In response to this research need, this study aims to examine spatial and temporal trends in soil erosivity across southern Africa and its different rainfall regions for the period 2000–2023 using monthly data of regional rainfall patterns. Based on this, the Standardized Precipitation Index (SPI), PCI, and MFI values are calculated. In detail, this paper (1) describes the rainfall climatology of the study area and the datasets used to analyze this; (2) presents the results of the study, including relationships between SPI, PCI, and MFI values in arid, semiarid, subhumid and humid regions of southern Africa and their variability; and (3) discusses these results in the context of rainfall and environmental variability across the country. Limitations with this approach, as applied to dryland areas in particular, are then identified. The outcomes of this study have implications for predicting soil erosion patterns under climate change for regions with variable hydrological regimes and are of relevance to farmers, policymakers, risk, and environmental managers, and conservationists seeking to predict the impacts of climate change on land surface properties.

2. Materials and Methods

2.1. Study Area

Southern Africa in this study broadly corresponds to the region south of ~22° S and includes South Africa (with Lesotho and eSwatini) and the southern parts of Namibia,

Botswana, Zimbabwe, and Mozambique (Figure 1a). Here, the geographical focus is specifically on South Africa (1.22 million km^2), set in this wider regional context. Annual rainfall in South Africa ranges from <1100 mm in the east to >350 mm in the west of the country; thus, there is a pronounced precipitation gradient. This arises as a result of the different moisture sources available from the east (Indian Ocean), west (Atlantic Ocean), and south (Southern Ocean) [43], and where coastal upwelling influences the moisture transport by air masses inland [44]. This region is also strongly affected by El Niño climate cycles that lead to much lower rainfall during strong El Niño events, and this was responsible for the significant drought experienced in the Western Cape Province of South Africa in 2015–16 [45]. Annual rainfall totals can be used to distinguish four broad rainfall regions in South Africa, corresponding to arid, semiarid, subhumid, and humid from west to east, respectively (Figure 1b). The methods used in the identification of these rainfall regions are described in Section 2.2.

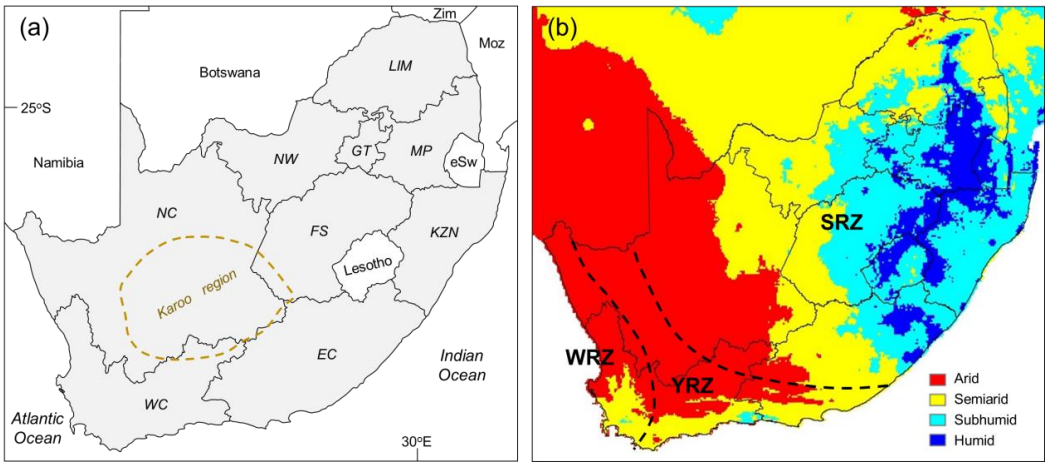


Figure 1. The location of the study area and sites mentioned in the text. (**a**) Countries within the southern Africa region (South Africa is shaded in grey). Moz = Mozambique; Zim = Zimbabwe; and eSw = eSwatini. Provinces within South Africa are as follows: LIM = Limpopo; GT = Gauteng; NW = Northwest; NC = Northern Cape; WC = Western Cape; EC = Eastern Cape; FS = Free State; KZN = KwaZulu-Natal; and MP = Mpumalanga. The Karoo region is circled within the brown line. (**b**) The rainfall regions of South Africa (arid, semiarid, subhumid, humid), as identified in this study, are mapped for the 'normal' year 2000 according to their annual rainfall values (see definitions in Section 2.2), SRZ = summer rainfall zone; YRZ = year-round rainfall zone; and WRZ = winter rainfall zone (from [41]), with their boundaries indicated by the thick dashed lines.

Rainfall seasonality is also a distinctive characteristic of South Africa's climate, whereby the eastern two-thirds of the country falls within the summer rainfall zone (SRZ), the western coastal fringe of the country within the winter rainfall zone (WRZ), and the transition between the two within the year-round rainfall zone (YRZ) (Figure 1b) [41,42]. Interior parts of the country within the YRZ exhibit relatively uniform rainfall patterns, whereas there is more irregular rainfall in the areas of the SRZ and WRZ [42]. In addition, some rainfall trends over recent decades can also be identified in different parts of the county. In the Karoo region, in the interior of South Africa (Figure 1a), rain gauge data from eight stations between 1936 and 2018 showed an increasing rainfall trend of 10 mm/decade [46]. In Gauteng Province in northeast South Africa, rainfall patterns between 1997 and 2009 showed an increasing late summer rainfall trend, and this coincided with more frequent extreme rain events during this season [47]. In the KwaZulu-Natal Province, historical and instrumental data on river flooding from 1836 to 2022 show how flooding frequency (based on cyclonic rainfall derived from the Indian Ocean) has doubled throughout the 20th century [48].

Rainfall patterns in South Africa have been used in some studies to evaluate patterns of erosivity [17,40], but these mainly highlight the influence of slope properties (altitude, steepness) [17,49] rather than the role of seasonal or event-scale precipitation events that are known to be a strong driver of erosivity throughout Africa as a whole [33].

2.2. Datasets and Analytical Methods Used

In this study, combined rain gauge and remote sensing data on rainfall patterns were derived from the Climate Hazard group InfraRed Precipitation with Stations (CHIRPS) gridded database for the period 1981 to present (available from https://data.chc.ucsb.edu/products/CHIRPS-2.0/ accessed on 29 August 2024). In detail, RFE2 is a composite (satellite and rain gauge) product produced by NOAA and presents decadal-scale rainfall data across Africa at 0.1° × 0.1° spatial resolution (available from https://earlywarning.usgs.gov/fews/product/48 accessed on 29 August 2024). From this dataset, we extracted monthly rainfall data for the study area for each year from 2000 to 2023. Across this time period, annual average rainfall across the region showed an overall slightly declining trend (Figure 2), although the 23-year period of analysis is too short to identify whether or not this represents any systematic change in rainfall climatology.

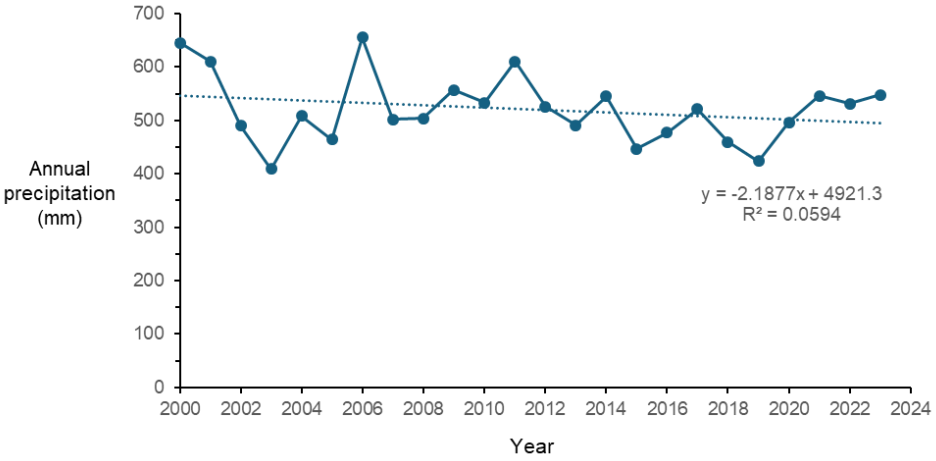


Figure 2. Trend of annual average precipitation across the southern Africa study area, 2000–2023.

Based on the CHIRPS dataset, we then identified four rainfall regions across southern Africa according to their annual total rainfall where broadly following UNEP convention [50], rainfall in the range 0–300 mm yr^{-1} was classified as arid, 301–600 mm yr^{-1} as semiarid, 601–800 mm yr^{-1} as subhumid, and >801 mm yr^{-1} as humid (Figure 1b). This was carried out for each year from 2000 to 2023. The reason for this classification was to characterize the typical rainfall properties of different localities in the study area and throughout the time period 2000–23.

The next step was to identify the wettest and driest years across southern Africa in this period using the Standardized Precipitation Index (SPI) [51]. The SPI is based on the comparison of annual rainfall for each year with the average annual rainfall across the entire period, which in this study is 2000–23. From this, anomalously wet and dry years are identified, defined here where the annual rainfall is +1.5 standard deviation (SD) and −1.5 SD from the mean value, respectively (Figure 3). Based on this definition, the two wettest years identified for the study area were 2000 and 2007, and the two driest years were 2003 and 2019. 'Normal' or average years were identified where SPI values were near zero; for the purpose of comparison with the extreme rainfall years, the normal years used here were taken to be 2010 and 2023 (Figure 4). SPI analysis was then undertaken for annual rainfall within each of the four rainfall regions. It should also be noted that the SPI has been previously used in South Africa to identify anomalously wet/dry years [1].

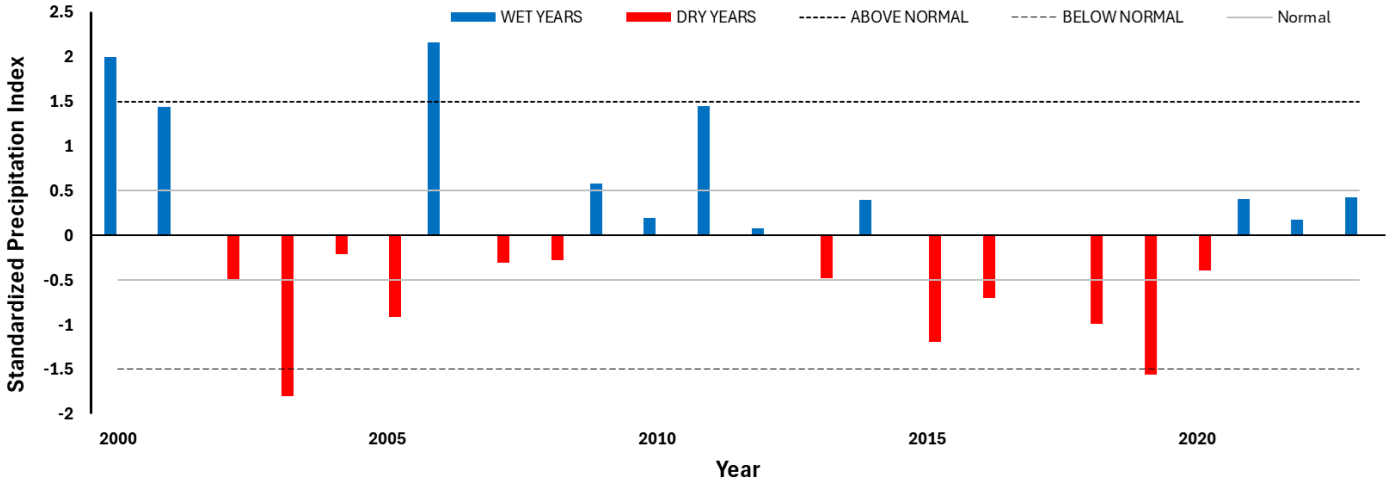


Figure 3. Standardized Precipitation Index values for annual rainfall across southern Africa for the period 2000 to 2023.

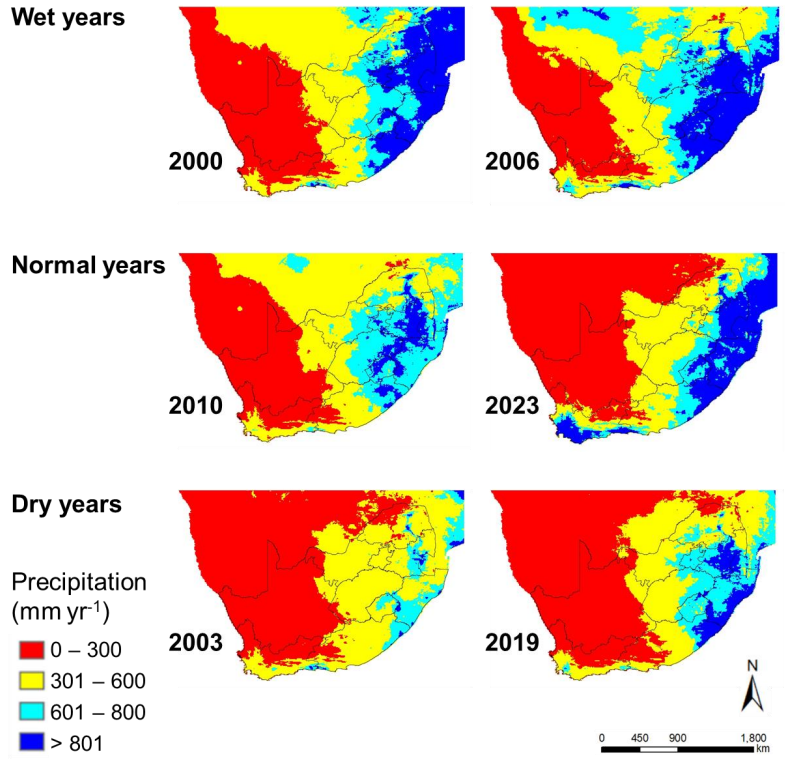


Figure 4. Spatial patterns of the four rainfall regions in southern Africa for the two wettest, two driest, and two 'normal' years.

Based on monthly rainfall values, the precipitation concentration index (PCI) was calculated as follows:

$$PCI = 100 \sum_{i=1}^{12} \left(\frac{P_i^2}{P^2} \right)$$

where P is precipitation, and P_i represents precipitation values for a single month [52]. PCI values reflect the distribution of monthly rainfall values with respect to rainfall received throughout the year. Thus, PCI values and their interpretation can be classified according to uniform rainfall conditions (PCI values of <10), including moderately seasonal (10–15), seasonal (15–20), highly seasonal (20–50), and irregular (50–100). Botai et al. [42] also calculated seasonal PCI values across South Africa for the period 1998–2015.

In order to calculate erosivity, various indices were used and derived from the monthly rainfall patterns. The Fournier erosivity index (FI) is calculated as follows:

$$FI = \frac{P_i^2}{P}$$

where FI is the Fournier index values; P_i is the monthly rainfall depth in i month; and P is the annual rainfall. In addition, the modified Fournier index (MFI) was calculated as follows:

$$MFI = \frac{\sum_{i=1}^{12} P_i^2}{P}$$

where MFI values are classified into very low erosivity (values of 0 to 60), low erosivity (60 to 90), moderate erosivity (90 to 120), high erosivity (120 to 160), and very high erosivity (>160) [53]. A raster tool was developed to calculate erosivity and seasonality values using the MFI and PCI equations, respectively.

In addition to values for the entire study area, PCI and MFI values were also calculated for the four rainfall regions, as identified through the SPI analysis. The purpose of this step was (1) to consider whether there are identifiable differences in rainfall seasonality between the different regions as reflected by PCI values and (2) to identify if any rainfall seasonality then influences the calculated erosivity values through the MFI. The latter may potentially be the case, as the WRZ and YRZ mainly include arid and semiarid regions (according to annual rainfall values, Figure 1b), whereas the SRZ has higher rainfall overall and spans all rainfall regions. If different seasonal rainfall patterns give rise to different erosivity values, then this is of concern to land managers and other user communities. The overall workflow employed in this study is summarized in Figure 5.

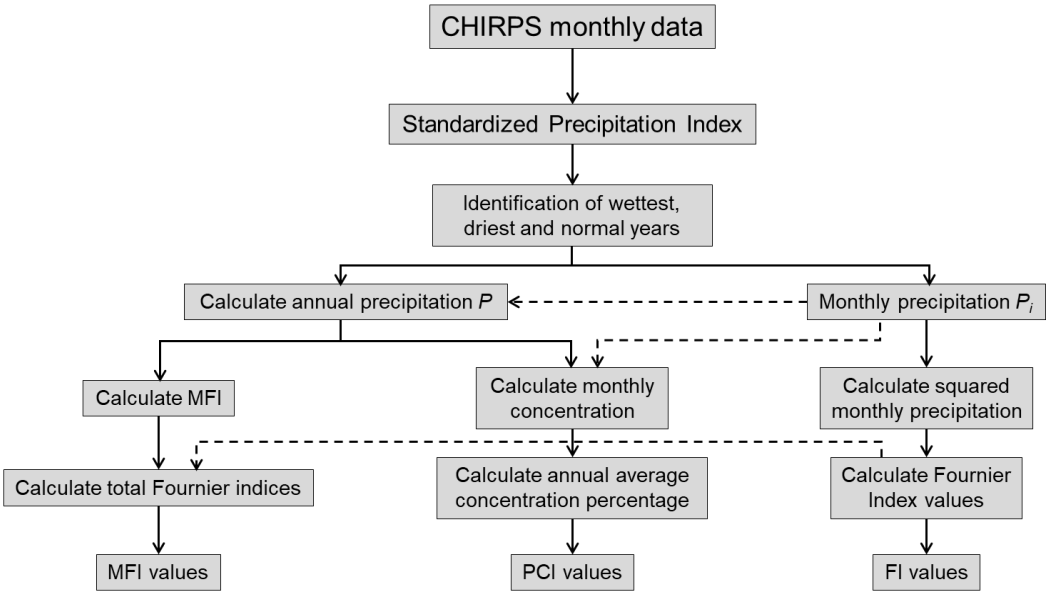


Figure 5. The raster analysis model workflow used in this study.

3. Results and Interpretation

3.1. SPI Values for the Different Rainfall Regions

SPI values across the entire region are used herein to identify wet, dry, and normal rainfall years (Figure 3). In detail, there have been differences in wet and dry anomaly years across the different rainfall regions (Table 1). For some years, like 2000, there are antiphase anomalies with dry areas, particularly dry and wet areas, and particularly wet areas. This is also seen in 2017. In other years, anomalies are seen in all areas, such as 2003 (dry), 2015 (dry), 2018 (dry), 2019 (dry), and 2023 (wet). The most likely reason behind these spatial patterns is synoptic circulation patterns and the role of El Niño [1,7] (see Section 3.3).

The apparent antiphase relationship between the wetter (east) and drier (west) parts of southern Africa has been considered previously and interpreted with respect to these major drivers [10,54].

Table 1. SPI anomaly values for the different rainfall regions identified in this study, 2000–23. Wet years (+1.5 SD) are shaded blue and dry years (−1.5 SD) are shaded gold. Values for the entire southern Africa region are presented in Figure 3.

Year	Arid Region	Semiarid Region	Subhumid Region	Humid Region
2000	−1.04	0.04	2.56	1.65
2001	1.53	2.04	0.89	0.83
2002	0.38	0.04	−0.40	0.06
2003	−1.20	−0.85	−1.76	−1.58
2004	−0.41	−1.33	−0.72	0.22
2005	0.41	−0.18	−0.59	−0.37
2006	1.15	1.96	0.77	2.12
2007	−0.73	−0.23	0.22	−0.48
2008	1.43	0.09	−0.58	0.15
2009	1.72	0.40	0.37	1.20
2010	−0.23	−0.49	−0.61	−0.45
2011	0.71	1.87	2.06	0.40
2012	0.19	0.00	0.83	1.10
2013	0.37	−0.69	−0.31	−0.35
2014	1.04	0.40	0.02	−1.40
2015	−1.01	−0.23	−0.59	−1.94
2016	0.08	−1.29	−0.95	−0.57
2017	−1.60	−0.77	0.28	0.28
2018	−1.08	−0.76	−0.78	−1.11
2019	−1.60	−1.84	−1.34	−0.81
2020	−0.49	0.06	−1.00	−0.45
2021	0.16	−0.37	0.09	−0.06
2022	−0.98	1.36	0.61	1.32
2023	1.20	0.75	0.94	0.22

3.2. PCI and MFI Variability in the Study Area

The proportion of the study area that is classified under the four rainfall classes in the wet, dry, and normal years examined is shown in Table 2. These results show that there is high variability in this proportion in all classes. Not surprisingly, humid areas and arid areas achieve their greatest extent under wet and dry years, respectively. However, even under wet years, arid and semiarid areas collectively represent between ~40 and 70% of the total study area, increasing to ~80–90% in dry years. This categorically confirms southern Africa as a dryland region [43] and possibly the overall drying trend identified in the regional rainfall record (Figure 2). The high variability in all classes also underlies problems arising from the erratic spatio-temporal nature of southern African rainfall [45] with respect to hazard and risk management [55].

The calculated PCI and MFI values for the different rainfall regions and years are presented in Table 3. The mean PCI values fall within the range for seasonal rainfall for all but two cells in the table; thus, "seasonality" is a major property of southern African rainfall [38,41]. However, the range of values recorded across different data points within all regions spans uniform to highly erratic rainfall behaviour. The range of PCI values is particularly high for wet years in arid regions, which may potentially indicate more erratic (extreme) rainfall events in these regions, such as through localized but high-magnitude thunderstorms [56]. It may also suggest the westward migration of the boundary between the SRZ and YRZ in these wet years. By contrast, humid regions have much lower PCI variability under all conditions and, therefore, may be considered more climatologically stable. MFI values are much more variable throughout. The mean MFI values for arid regions record very low erosivity and with a very narrow value range (between 27 and 33) under all rainfall conditions; semiarid regions show low erosivity; subhumid regions mainly show moderate erosivity; and humid regions mainly show very high erosivity. The range of mean values generally increases with increased rainfall. Although the dependent relationship of MFI to rainfall may be expected [40], it is notable that extremely high MFI values are recorded throughout (except for arid regions) and under all rainfall conditions. The mean MFI values calculated in this study (Table 3, range of 27 to 219 across the study area) are comparable to those from other regions in Africa that are also affected by seasonal rainfall patterns. For example, in Rwanda, MFI values are in the range of 115–175 [37]; in East Africa, it is 30–270 [27]; and in Ethiopia, it is 101–173 [36].

Table 2. The proportion of the total study area classified according to the four rainfall regions in wet, normal and dry years.

Rainfall Conditions	Year	Rainfall Region	Area (% of Total)
Wet years	2000	Arid	32.77
		Semiarid	35.40
		Subhumid	13.24
		Humid	18.59
	2006	Arid	20.97
		Semiarid	27.54
		Subhumid	34.11
		Humid	17.38
Normal years	2010	Arid	34.09
		Semiarid	41.62
		Subhumid	18.51
		Humid	5.78
	2023	Arid	52.13
		Semiarid	23.90
		Subhumid	8.86
		Humid	15.10
Dry years	2003	Arid	46.91
		Semiarid	40.93
		Subhumid	7.04
		Humid	5.13
	2019	Arid	52.51
		Semiarid	28.63
		Subhumid	10.40
		Humid	8.46

Table 3. PCI and MFI results for the four rainfall regions and for the wet, normal, and dry years identified in the SPI analysis. Cells are colour-coded according to the categories of PCI (Figure 6) and MFI values (Figure 7).

Rainfall Conditions	Year	Rainfall Region	PCI Value					MFI Value				
			Min	Max	Range	Mean	SD	Min	Max	Range	Mean	SD
Wet years	2000	Arid	8.83	52.42	43.59	19.26	7.15	2.76	111.11	108.34	33.37	18.66
		Semiarid	8.73	37.13	28.40	18.14	4.71	28.07	164.96	136.89	83.27	24.14
		Subhumid	10.62	30.97	20.36	16.68	5.15	69.94	237.91	167.97	116.85	38.01
		Humid	10.56	29.70	19.14	16.76	4.15	89.61	899.17	809.56	178.49	65.33
	2006	Arid	9.38	54.75	45.37	17.12	4.63	4.14	97.02	92.88	29.49	15.72
		Semiarid	9.60	33.69	24.08	17.90	3.77	29.34	186.22	156.87	84.17	24.89
		Subhumid	9.80	31.50	21.70	19.07	2.96	60.02	219.51	159.48	133.78	22.85
		Humid	9.71	28.57	16.05	16.05	3.28	81.51	423.82	342.31	152.40	35.57
Normal years	2010	Arid	8.95	40.55	31.60	17.22	5.81	2.36	100.64	98.27	29.29	18.85
		Semiarid	9.28	38.06	28.77	17.79	3.56	28.27	167.50	139.23	81.35	20.33
		Subhumid	9.84	27.22	17.38	15.94	2.50	59.62	201.75	142.13	110.36	17.83
		Humid	9.72	27.36	17.64	15.42	1.71	89.94	285.04	195.10	137.43	20.64
	2023	Arid	8.75	47.13	38.38	16.42	4.19	1.94	106.16	104.22	27.28	17.29
		Semiarid	9.17	33.45	24.29	16.13	4.07	29.50	165.88	136.37	68.71	20.97
		Subhumid	9.07	29.27	20.20	15.13	4.41	56.04	218.82	162.78	104.72	30.91
		Humid	9.23	32.90	23.67	18.24	5.39	77.29	566.04	488.75	188.31	74.52
Dry years	2003	Arid	8.70	41.16	32.46	16.21	4.14	2.42	70.02	67.60	29.38	15.20
		Semiarid	9.49	23.44	13.95	15.95	2.71	31.40	139.15	107.75	67.10	15.41
		Subhumid	9.80	26.23	16.44	14.31	2.88	61.97	205.09	143.12	96.55	20.80
		Humid	9.68	25.25	15.57	16.25	3.16	80.10	447.88	367.78	165.34	49.11
	2019	Arid	8.61	39.99	31.38	17.88	4.59	1.90	98.05	96.14	29.64	18.12
		Semiarid	8.83	39.24	30.40	18.41	3.87	26.63	216.71	190.08	77.92	20.99
		Subhumid	8.96	35.54	26.58	16.93	3.15	54.88	268.76	213.87	116.35	22.03
		Humid	9.32	33.67	24.34	20.19	5.69	90.91	769.51	678.59	219.83	99.51

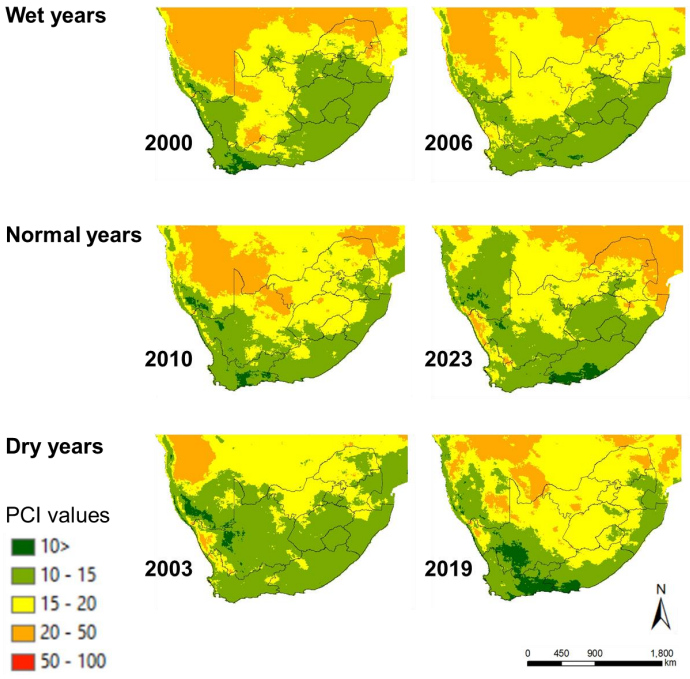


Figure 6. Calculated PCI values across southern Africa for the two wet, 'normal', and dry years examined across the time series of this study. Note that the highest PCI category values are not found in the study area in these years.

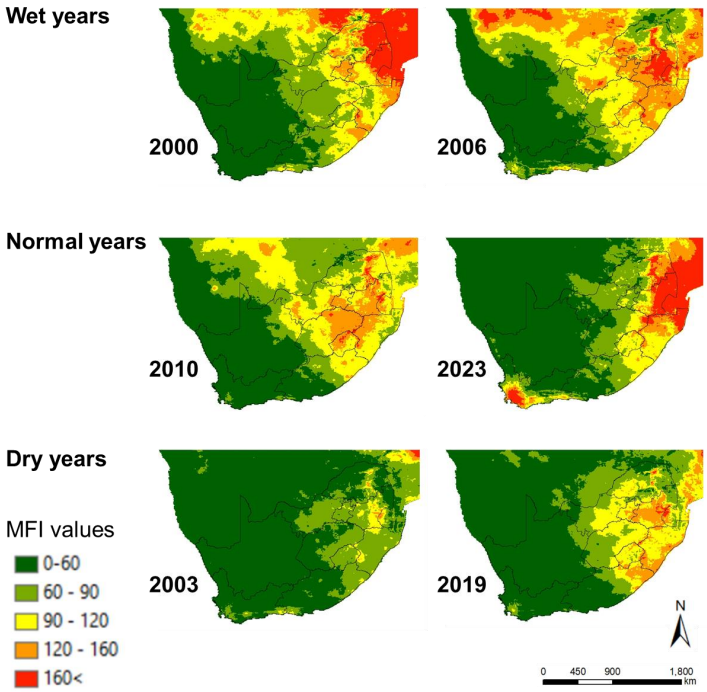


Figure 7. Calculated MFI values across southern Africa for the two wet, 'normal', and dry years examined across the time series of this study.

The spatial patterns of PCI and MFI values across the study area can also be examined, and these are shown in Figures 6 and 7, respectively. PCI values have highly variable patterns, both within and between overall wet and dry years. Low PCI values indicating uniform rainfall patterns show the greatest spatial variability, and this category of values appears to migrate across the south coast of South Africa and broadly reflect the zonation of the YRZ. This has been noted in previous studies [57,58]. It is also notable that highly seasonal rainfall is suppressed under dry years, which is indicative of the failure of seasonal rains. These spatial patterns may also mirror some regional changes in rainfall properties identified by Kruger and Nxumalo [59] based on the analysis of data from weather stations across South Africa for the period 1921–2015. That study shows, across this time period, increases in total annual rainfall in northeast and southern South Africa, increases in summer rainfall, and increases in daily rainfall intensity. These longer-term patterns may give rise to long-term changes in erosivity.

The spatial patterns of MFI values are presented in Figure 7. The majority of the study area falls under very low erosivity conditions in all years, especially in dry years where, of course, rainfall totals are lower. The regions affected by moderate or greater erosivity, irrespective of wet or dry years, are located in the east of the area and, thus, within the SRZ and match the patterns of annual rainfall from which they are derived (Figure 4). It is notable that areas of very high erosivity vary in proportion and location between the time periods examined (Table 3), are found mainly in the northeast of the region, and are likely associated with extreme and intense rainfall events found in this area. For example, a tropical depression from the Indian Ocean in February 2000 (a wet year) resulted in extreme rainfall (24 h total of 300–500 mm, return period of <200 years) in southern Mozambique and NE South Africa [60]. The imprint of this event may be that which is recorded in the image for the year 2000. Despite being categorized here as a 'normal' year overall, 2023 included the category 5 Cyclone Freddy (February–March 2023) that made landfall in southern Mozambique and resulted in intense rainfall (<600 mm) and flooding in this area and in Malawi [61]. This can account for the very high erosivity values seen in this region in 2023. Under overall dry conditions, erosivity is much lower throughout, which may be due, in part, to a changing frequency of tropical cyclones to the east of the study area but also due to other factors such as blocking highs and the influence of El Niño.

3.3. Seasonality of Rainfall and Resulting PCI and MFI Values

In detail, the seasonal patterns of rainfall received in the four rainfall zones show some notable differences (Table 3, Figure 8) that broadly reflect their spatial position with respect to the WRZ, YRZ, and SRZ. For example, arid regions within the WRZ have the greatest rainfall variability in that season (austral winter months JJA). The greatest difference in rainfall is found in the southern hemisphere summer season months (DJF), and the lowest difference is in the autumn months (fall) (JJA) (Figure 8). Humid/subhumid areas are, by definition, wetter than arid areas. El Niño periods are associated with lower rainfall in semiarid areas during the summer; there is less impact on rainfall in other areas or in other seasons [62,63]. These types of spatial patterns in rainfall reflect synoptic-scale circulation patterns and the interplay between weather systems from different source areas [42,64]. There is no clear trend in any changes in rainfall seasonality per region over the time series examined (Figure 8), but other studies based on different records have identified some persistence in earlier winter rains within the WRZ [65], the lengthening of the rain season within the WRZ [11], shifts in the position of the SRZ/YRZ boundary [58], and increased rainy days/rain intensity in the SRZ [66]. This diversity of evidence certainly suggests some reconfiguration of synoptic circulation patterns over southern Africa in recent decades, likely reflecting larger, hemispheric-scale changes.

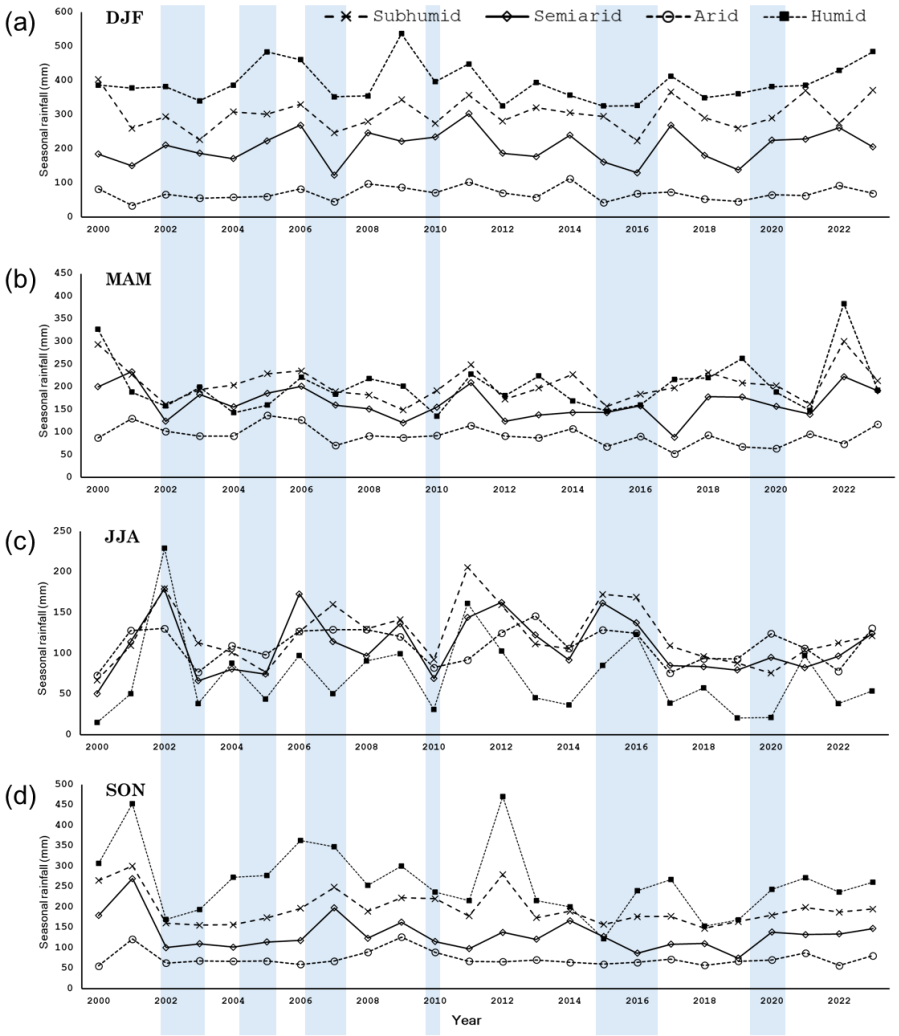


Figure 8. Seasonality of rainfall patterns received in the different rainfall zones in southern Africa, 2000–2023, where (**a**) summer season DJF, (**b**) autumn/fall MAM, (**c**) winter JJA, (**d**) spring SON. For comparison, El Niño events (blue shaded zones) are shown based on Southern Oscillation Index values (from https://www.ncei.noaa.gov/access/monitoring/enso/soi, accessed on 30 August 2024).

The MFI categories are very different between the climate zones, with arid areas exclusively low and humid areas much more variable but mainly high/very high (Figure 9). Semiarid and subhumid area values fit between these end members. Average PCI values are remarkably similar throughout and across all rainfall regions. There is not a close match between SPI variability in different regions (Table 1) and the PCI values. The correlation coefficients of these relationships are shown in Table 4. Overall, the highest positive correlations are with the MFI in the arid climate zone during autumn and winter. This may reflect the seasonality of rainfall in this region (in the WRZ). In the subhumid and humid zones, high positive relationships are found with both MFI and PCI in the spring (SON) and summer (DJF) and negative relationships in the winter (JJA). Thus, the seasonality of MFI and PCI is particularly pronounced in this area. This is further shown in Figure 10, where the subhumid region shows a higher correlation coefficient between MFI and PCI compared to the other climate regions. Potential reasons why there is a weaker relationship between these variables in arid, semiarid, and humid areas are discussed below.

Table 4. Correlation coefficients of rainfall properties (MFI, PCI) by season in the different rainfall zones analyzed. DJF = southern hemisphere summer; MAM = southern hemisphere autumn (fall); JJA = summer hemisphere winter; and SON = southern hemisphere spring.

Arid						
	MFI	***PCI***	***DJF***	***MAM***	***JJA***	***SON***
MFI	1					
PCI	0.394	1				
DJF	0.036	−0.442	1			
MAM	0.774	0.264	0.133	1		
JJA	0.584	0.251	−0.207	0.188	1	
SON	0.568	0.015	−0.074	0.209	0.241	1
Semiarid						
	MFI	***PCI***	***DJF***	***MAM***	***JJA***	***SON***
MFI	1					
PCI	0.365	1				
DJF	0.453	0.286	1			
MAM	0.391	−0.284	−0.002	1		
JJA	0.103	−0.395	0.033	−0.155	1	
SON	0.491	−0.053	−0.210	0.283	−0.028	1
Subhumid						
	MFI	PCI	DJF	MAM	JJA	SON
MFI	1					
PCI	0.793	1				
DJF	0.675	0.630	1			
MAM	0.567	0.432	0.206	1		
JJA	−0.320	−0.554	−0.139	−0.376	1	
SON	0.576	0.262	0.072	0.113	−0.023	1
Humid						
	MFI	PCI	DJF	MAM	JJA	SON
MFI	1					
PCI	0.335	1				
DJF	0.549	0.376	1			
MAM	0.443	−0.099	0.168	1		
JJA	−0.240	−0.417	0.041	−0.312	1	
SON	0.640	0.018	0.140	−0.003	−0.058	1

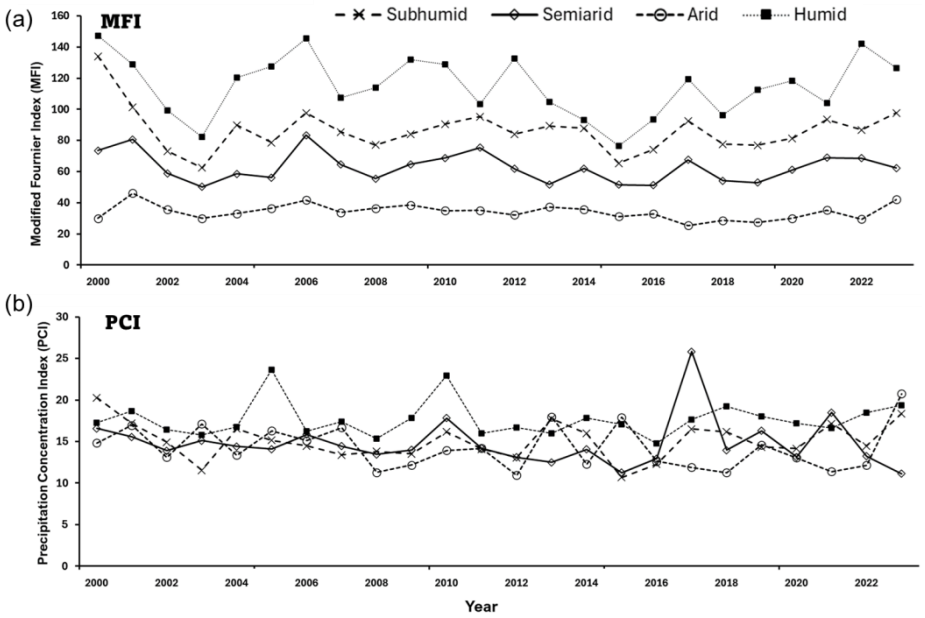


Figure 9. Variations in (**a**) MFI and (**b**) PCI values in the different rainfall zones in southern Africa, 2000–2023.

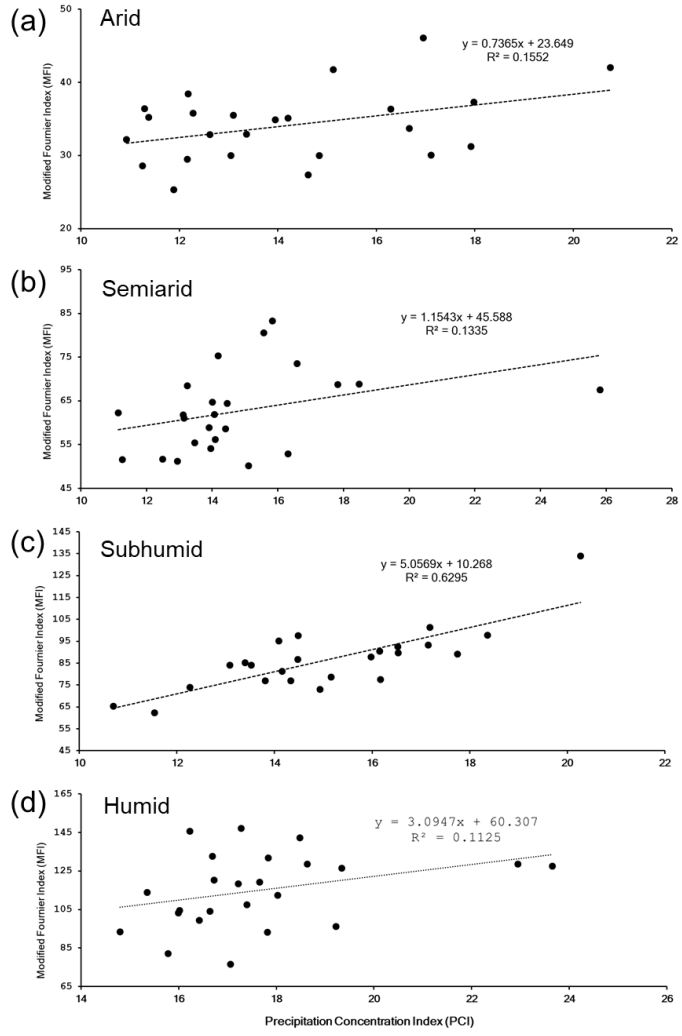


Figure 10. Relationships between PCI and MFI values across southern Africa for the different rainfall regions. (**a**) Arid, (**b**) semiarid, (**c**) subhumid, (**d**) humid.

4. Discussion

The variable rainfall regimes found across southern Africa give rise to certain spatial patterns in PCI (Figure 6) and erosivity (Figure 7), but this variability is hidden at the scale of national-level assessments of rainfall erosivity [40]. Equally, more local-scale studies highlight the role of soil properties and slope aspects as controls on erosivity [17,67], whereas these are not resolved at a regional scale. In this study, the coarse-resolution satellite data used may have influenced the dominance of very low and low MFI values found across the region (Figure 7), where the data resolution may not capture detailed environmental or climatic variability. Likewise, the temporal resolution of the dataset does not allow for event-scale analysis of rainfall erosivity (i.e., calculation of EI_{30} values), which has been the focus of some more localized studies [68,69]. Nonetheless, analysis of rainfall and MFI seasonality (Figures 8–10, Table 4) hints at the dynamic and changing nature of rainfall patterns and zones in southern Africa. The overall stability of PCI values over interannual timescales (Figure 9b) hides greater complexity at seasonal timescales (Table 4), where the highest correlation coefficients are found in the subhumid zone (falling within the SRZ). This is confirmed by the highest R^2 value being observed here between PCI and MFI (Figure 10c). It is also notable that MFI values in arid and humid areas are highest in the 'transition' seasons of spring and autumn. Although spatial or temporal shifts in rainfall seasonality (and, therefore, erosivity) cannot be resolved in this study, the impacts of any changes will be seen in land surface processes and properties, including vegetation, soil/sediment export, and hazard risk [19].

In detail, low erosivity values in the west of the study area arise as a result of low rainfall totals and low seasonality (Figure 7). However, this belies the high land surface erosion potential that can still take place in these arid and semiarid environments. Here, (i) rainfall is highly episodic, and event-scale rainfall tends to be very intense (likely with high EI_{30} values, although this has not been tested), but that event-scale rainfall is not captured in monthly rainfall totals [24,70]; (ii) low average rainfall totals mean low vegetation cover and so the erosive effects of rainfall on the land surface will be much greater than in areas with higher vegetation cover; and (iii) dry land surface is also more strongly affected by wind erosion, which can also contribute to surface erosion and sediment export [71]. For these reasons, predictive erosivity models have limitations when they are applied to semiarid areas with strongly seasonal or event-scale climatic regimes [28,72], as evidenced by the wide range of MFI values calculated for arid regions in this study (Table 3). However, these problems associated with erosivity in arid areas are not well described in the literature, nor is the interplay between rainfall, vegetation, land surface properties, and erosivity well understood [73,74]. By contrast, moderate and high values of erosivity are concentrated to the east of the study area (Figure 7). These areas, such as Limpopo, Mpumalanga, and KwaZulu-Natal provinces in South Africa, are hotspots of historical and present soil erosion [75–78] that can be interpreted to arise as an outcome of the region's high rainfall. However, high soil erosion potential across the study area is also affected by high stocking density, overgrazing, and land degradation, and these are independent of the rainfall regime [79,80]. Thus, the outcomes of erosion on the land surface—such as land degradation—are not the result of rainfall alone, highlighting the limitations of predictive erosivity models in being able to identify the regions at risk from such environmental hazards.

The Fournier index is deterministically associated with certain rates of soil loss that, in turn, result in certain erosion risk classes being identified [53,74]. Although the Fournier index deals specifically with the monthly rainfall regime, the likelihood of soil erosion taking place will vary according to the physical properties of the land surface, corresponding to the erodibility factor *K* identified in the USLE [19,31,81]. This means that MFI values themselves (Figure 7) and their spatial and temporal expressions in different rainfall zones (Figures 7 and 9) and over time (Figure 7) might not be able to explain the soil erosion risk or catchment sediment yield [26].

Figure 11 presents a model describing some of these relationships, especially applicable to arid and semiarid areas where rainfall erosivity is a particular issue for land degradation and, thus, where predictive models of erosivity work least well [17,20,33].

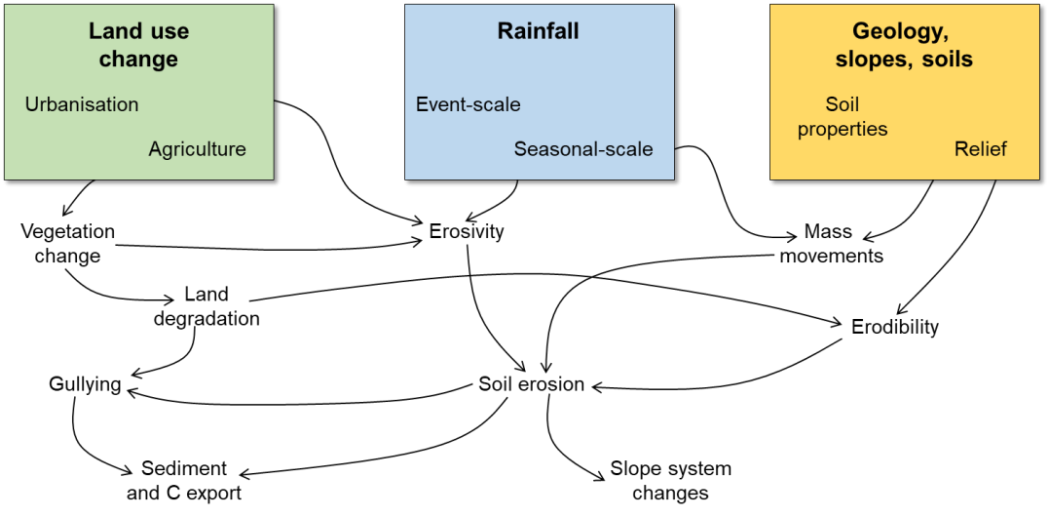


Figure 11. Interconnections between environmental and climatic factors and the processes that result in erosivity risk to the land surface.

Soil erosion is a significant contemporary issue in southern Africa, and several studies have examined the distribution of areas susceptible to erosion risk [82]. For example, based on MODIS satellite data, Le Roux et al. [16] estimated that 50% of South Africa's area is under moderate-to-severe potential erosion risk based on the USLE. Likewise, spatial mapping from SPOT satellite data shows the distribution of erosional gullies that are concentrated in Eastern Cape and KwaZulu-Natal provinces of South Africa [83]. These areas correspond to areas of unconsolidated Quaternary colluvium [84] as well as intense agriculture [85] and are, thus, sensitive to changes in rainfall seasonality in this region, which are located towards the margin of the SRZ. Examining these types of localities, where rainfall shows greater interannual and seasonal variability [41,48], can better explore the land surface and rainfall controls on erosivity. For example, using higher-resolution rainfall data, such as 3 h data from the TMPA, may give a more accurate assessment of the impacts of event-scale rainfall [33]. However, such data may be inappropriate or too computer-intensive for larger regional and longer temporal scales.

Several limitations of the study can be identified. Although this study adopts a consistently applied approach covering the entire southern African region and uses medium-scale spatial and temporal resolution data in order to conduct this, any smaller-scale variability of rainfall events and, thus, erosivity is hidden. Feedback related to land surface properties, land use, and agriculture (Figure 11) is also not explored in detail. The role of ongoing climate change (e.g., increasing aridity or more variable rainfall events) was not examined, and this may require a larger dataset. The effects of climate cycles, such as El Niño on erosivity patterns, were also not examined; however, they have been identified and discussed (Figure 8). These limitations can also help identify possible future research directions. For example, seasonal-scale variations in rainfall values and erosivity between different rainfall regions could well be a fingerprint of climate change, so more detailed quantitative analysis is needed. Future work may also involve applying rainfall data to a land surface model, including slope, soils, and land use, in order to predict erosivity and sediment yield based on the calculated *R*-factor of the USLE. This approach can help understand the interconnections between rainfall seasonality and land surface properties (Figure 11). This information can also help guide land conservation strategies, including reducing the soil erosion risk.

5. Conclusions

This study highlights the application and limitations of using satellite datasets for erosivity modelling across large spatial scales, such as all of southern Africa. Calculating rainfall erosivity is important for evaluating the impacts of annual, seasonal, and event-scale rainfall patterns on the land's surface. However, this study shows that there are significant differences in both annual averaged and seasonal erosivity patterns in the different rainfall regions of southern Africa that are a reflection of regional synoptic climatology. There are also feedbacks within these regions that affects erosivity, including wind erosion (in dry seasons), vegetation cover, slope/elevation, and agriculture (Figure 11). These can influence the volume of land surface erosion and sediment export independent of rainfall itself.

In addition, climate models predict how future changes in rainfall patterns across southern Africa—both spatially and seasonally—are likely to result in changes in erosivity [86]. However, these impacts are, as yet, unknown, posing uncertainty in predicting soil erosion and land degradation risks. Likewise, an increase in event-scale rainfall intensity (e.g., EI_{30} values) that is often a typical outcome of climate change can also lead to higher soil erosion and gullying rates and sediment and carbon export, especially over degraded land surfaces [87].

Author Contributions: Conceptualization, M.A.M.A.E. and J.K.; methodology, M.A.M.A.E.; formal analysis, M.A.M.A.E.; writing—original draft preparation, J.K.; writing—review and editing, M.A.M.A.E. and J.K.; visualization, M.A.M.A.E. and J.K. All authors have read and agreed to the published version of the manuscript.

Funding: This research received no external funding.

Institutional Review Board Statement: Not applicable.

Informed Consent Statement: Not applicable.

Data Availability Statement: The original contributions presented in the study are included in the article, further inquiries can be directed to the corresponding author/s.

Conflicts of Interest: The authors declare no conflicts of interest.

References

1. Adeola, O.M.; Masinde, M.; Botai, J.O.; Adeola, A.M.; Botai, C.M. An Analysis of Precipitation Extreme Events Based on the SPI and EDI Values in the Free State Province, South Africa. *Water* **2021**, *13*, 3058. [CrossRef]
2. Ullah, A.; Pohl, B.; Pergaud, J.; Dieppois, B.; Rouault, M. Intraseasonal descriptors and extremes in South African rainfall. Part I: Summer climatology and statistical characteristics. *Int. J. Climatol.* **2022**, *42*, 4538–4563. [CrossRef]
3. Munzhedzi, L.; Mugari, E.; Nethengwe, N.S.; Gumbo, A.D. Trends in extreme rainfall and their relationship to flooding episodes in Vhembe district, South Africa. *Environ. Res. Commun.* **2024**, *6*, 095016. [CrossRef]
4. Ogwang, B.A.; Ongoma, V.; Shilenje, Z.W.; Ramotubei, T.S.; Letuma, M.; Ngaina, J.N. Influence of Indian Ocean dipole on rainfall variability and extremes over southern Africa. *Mausam* **2020**, *71*, 637–648.
5. Mpungose, N.; Thoithi, W.; Blamey, R.C.; Reason, C.J.C. Extreme rainfall events in southeastern Africa during the summer. *Theor. Appl. Climatol.* **2022**, *150*, 185–201. [CrossRef]
6. Rapolaki, R.S.; Blamey, R.C.; Hermes, J.C.; Reason, C.J.C. Moisture sources associated with heavy rainfall over the Limpopo River Basin, southern Africa. *Clim. Dyn.* **2020**, *55*, 1473–1487. [CrossRef]
7. Jury, M.R. A Survey of African Weather and Climate Extremes. *Climate* **2024**, *12*, 65. [CrossRef]
8. Botai, C.M.; Botai, J.O.; Zwane, N.N.; Hayombe, P.; Wamiti, E.K.; Makgoale, T.; Murambadoro, M.D.; Adeola, A.M.; Ncongwane, K.P.; de Wit, J.P.; et al. Hydroclimatic Extremes in the Limpopo River Basin, South Africa, under Changing Climate. *Water* **2020**, *12*, 3299. [CrossRef]
9. Makungo, R.; Mashinye, M.D. Long-term trends and changes in rainfall magnitude and duration in a semi-arid catchment, South Africa. *J. Water Clim. Chang.* **2022**, *13*, 2319. [CrossRef]
10. Cook, C.; Reason, C.J.C.; Hewitson, B.C. Wet and dry spells within particularly wet and dry summers in the South African summer rainfall region. *Clim. Res.* **2004**, *26*, 17–31. [CrossRef]
11. du Plessis, J.A.; Schloms, B. An investigation into the evidence of seasonal rainfall pattern shifts in the Western Cape, South Africa. *J. S. Afr. Inst. Civ. Eng.* **2017**, *59*, 47–55. [CrossRef]
12. Lehmann, J.; Mempel, F.; Coumou, D. Increased occurrence of record-wet and record-dry months reflect changes in mean rainfall. *Geophys. Res. Lett.* **2018**, *45*, 13468–13476. [CrossRef]

13. Kruger, A.C. Observed trends in daily precipitation indices in South Africa: 1910–2004. *Int. J. Climatol.* **2006**, *26*, 2275–2285. [CrossRef]
14. McBride, C.M.; Kruger, A.C.; Dyson, L. Changes in extreme daily rainfall characteristics in South Africa: 1921–2020. *Weather Clim. Extrem.* **2022**, *38*, 100517. [CrossRef]
15. Bradshaw, C.D.; Pope, E.; Kay, G.; Davie, J.C.S.; Cottrell, A.; Bacon, J.; Cosse, A.; Dunstone, N.; Jennings, S.; Challinor, A.; et al. Unprecedented climate extremes in South Africa and implications for maize production. *Environ. Res. Lett.* **2022**, *17*, 084028. [CrossRef]
16. Le Roux, J.J.; Morgenthal, T.L.; Malherbe, J.; Pretorius, D.J.; Sumner, P.D. Water erosion prediction at a national scale for South Africa. *Water SA* **2008**, *34*, 305–314. [CrossRef]
17. Phinzi, K.; Ngetar, N.S.; Ebhuoma, O. Soil erosion risk assessment in the Umzintlava catchment (T32E), Eastern Cape, South Africa, using RUSLE and random forest algorithm. *S. Afr. Geogr. J.* **2021**, *103*, 139–162. [CrossRef]
18. Vrieling, A.; Sterk, G.; de Jong, S.M. Satellite-based estimation of rainfall erosivity for Africa. *J. Hydrol.* **2010**, *395*, 235–241. [CrossRef]
19. Diodato, N.; Knight, J.; Bellochi, G. Reduced complexity model for assessing patterns of rainfall erosivity in Africa. *Glob. Planet Chang.* **2013**, *100*, 183–193. [CrossRef]
20. Panagos, P.; Borrelli, P.; Meusburger, K.; Yu, B.; Klik, A.; Lim, K.J.; Yang, J.E.; Ni, J.; Miao, C.; Chattopadhyay, N.; et al. Global rainfall erosivity assessment based on high-temporal resolution rainfall records. *Sci. Rep.* **2017**, *7*, 4175. [CrossRef]
21. Panagos, P.; Hengl, T.; Wheeler, I.; Marcinkowski, P.; Rukeza, M.B.; Yu, B.; Yang, J.E.; Miao, C.; Chattopadhyay, N.; Sadeghi, S.H.; et al. Global rainfall erosivity database (GloREDa) and monthly R-factor data at 1 km spatial resolution. *Data Brief* **2023**, *50*, 109482. [CrossRef] [PubMed]
22. Nyssen, J.; Vandenreyken, H.; Poesen, J.; Moeyersons, J.; Deckers, J.; Haile, M.; Salles, C.; Govers, G. Rainfall erosivity and variability in the Northern Ethiopian Highlands. *J. Hydrol.* **2005**, *311*, 172–187. [CrossRef]
23. Yin, S.; Xie, Y.; Nearing, M.A.; Wang, C. Estimation of rainfall erosivity using 5- to 60-minute fixed-interval rainfall data from China. *CATENA* **2007**, *70*, 306–312. [CrossRef]
24. Salako, F.K. Rainfall variability and kinetic energy in Southern Nigeria. *Clim. Chang.* **2008**, *86*, 151–164. [CrossRef]
25. Angulo-Martínez, M.; Beguería, S. Estimating rainfall erosivity from daily precipitation records: A comparison among methods using data from the Ebro Basin (NE Spain). *J. Hydrol.* **2009**, *379*, 111–121. [CrossRef]
26. Tamene, L.; Park, S.J.; Dikau, R.; Vlek, P.L.G. Analysis of factors determining sediment yield variability in the highlands of northern Ethiopia. *Geomorphology* **2006**, *76*, 76–91. [CrossRef]
27. Fenta, A.A.; Yasuda, H.; Shimizu, K.; Haregeweyn, N.; Kawai, T.; Sultan, D.; Ebabu, K.; Belay, A.S. Spatial distribution and temporal trends of rainfall and erosivity in the Eastern Africa region. *Hydrol. Process.* **2017**, *31*, 4555–4567. [CrossRef]
28. Meddi, M.; Toumi, S.; Assani, A.A. Spatial and temporal variability of the rainfall erosivity factor in Northern Algeria. *Arab. J. Geosci.* **2016**, *9*, 282. [CrossRef]
29. Hallouz, F.; Meddi, M.; Mahe, G.; Rahmani, S.E.A.; Zettam, A. Hybrid Analysis of Rainfall Erosivity in Northern Algeria: Integrating Empirical and Modeling Approaches. *Pure Appl. Geophys.* **2023**, *180*, 3995–4023. [CrossRef]
30. Wischmeier, W.H.; Smith, D.D. *Predicting Rainfall Erosion Losses—A Guide to Conservation Planning*; USDA Handbook 537: Washington, DC, USA, 1978.
31. Kinnell, P.I.A. Event soil loss, runoff and the Universal Soil Loss Equation family of models: A review. *J. Hydrol.* **2010**, *385*, 384–397. [CrossRef]
32. Haile, G.W.; Fetene, M. Assessment of soil erosion hazard in Kilie catchment, East Shoa, Ethiopia. *Land Degrad. Develop.* **2012**, *23*, 293–306. [CrossRef]
33. Vrieling, A.; Hoedjes, J.C.B.; van der Velde, M. Towards large-scale monitoring of soil erosion in Africa: Accounting for the dynamics of rainfall erosivity. *Glob. Planet. Chang.* **2014**, *115*, 33–43. [CrossRef]
34. Munka, C.; Cruz, G.; Caffera, R.M. Long term variation in rainfall erosivity in Uruguay: A preliminary Fournier approach. *GeoJournal* **2007**, *70*, 257–262. [CrossRef]
35. Elagib, N.A. Changing rainfall, seasonality and erosivity in the hyper-arid zone of Sudan. *Land Degrad. Develop.* **2011**, *22*, 505–512. [CrossRef]
36. Meshesha, D.T.; Tsunekawa, A.; Tsubo, M.; Haregeweyn, N.; Adgo, E. Evaluating spatial and temporal variations of rainfall erosivity, case of Central Rift Valley of Ethiopia. *Theor. Appl. Climatol.* **2015**, *119*, 515–522. [CrossRef]
37. Muhire, I.; Ahmed, F.; Abd Elbasit, M.M.M. Spatio-temporal variations of rainfall erosivity in Rwanda. *J. Soil. Sci. Env. Manag.* **2015**, *6*, 72–83.
38. Liebmann, B.; Bladé, I.; Kiladis, G.N.; Carvalho, L.M.V.; Senay, G.B.; Allured, D.; Leroux, S.; Funk, C. Seasonality of African Precipitation from 1996 to 2009. *J. Clim.* **2012**, *25*, 4304–4322. [CrossRef]
39. Nicholson, S.E.; Some, B.; McCollum, J.; Nelkin, E.; Klotter, D.; Berte, Y.; Diallo, B.M.; Gaye, I.; Kpabeba, G.; Ndiaye, O.; et al. Validation of TRMM and Other Rainfall Estimates with a High-Density Gauge Dataset for West Africa. Part II: Validation of TRMM Rainfall Products. *J. Appl. Meteorol.* **2003**, *42*, 1355–1368. [CrossRef]
40. Smithen, A.A.; Schulze, R.E. The spatial distribution in southern Africa of rainfall erosivity for use in the Universal Soil Loss Equation. *Water SA* **1982**, *8*, 74–78.

41. Roffe, S.J.; Fitchett, J.M.; Curtis, C.J. Classifying and mapping rainfall seasonality in South Africa: A review. *S. Afr. Geogr. J.* **2019**, *101*, 158–174. [CrossRef]
42. Botai, C.M.; Botai, J.O.; Adeola, A.M. Spatial distribution of temporal precipitation contrasts in South Africa. *S. Afr. J. Sci.* **2018**, *114*, 70–78. [CrossRef] [PubMed]
43. Dube, L.T. Climate of Southern Africa. *S. Afr. Geogr. J.* **2002**, *84*, 125–138. [CrossRef]
44. Jury, M.R. Climate trends across South Africa since 1980. *Water SA* **2017**, *43*, 297–307. [CrossRef]
45. Botai, C.M.; Botai, J.O.; de Wit, J.P.; Ncongwane, K.P.; Adeola, A.M. Drought characteristics over the Western Cape Province, South Africa. *Water* **2017**, *9*, 876. [CrossRef]
46. Harmse, C.J.; Du Toit, J.C.O.; Swanepoel, A.; Gerber, H.J. Trend analysis of long-term rainfall data in the Upper Karoo of South Africa. *Trans. R. Soc. S. Afr.* **2021**, *76*, 1–12. [CrossRef]
47. Dyson, L.L. Heavy daily-rainfall characteristics over the Gauteng Province. *Water SA* **2009**, *35*, 627–638. [CrossRef]
48. Grab, S.W.; Nash, D.J. A new flood chronology for KwaZulu-Natal (1836–2022): The April 2022 Durban floods in historical context. *S. Afr. Geogr. J.* **2024**, *106*, 476–497. [CrossRef]
49. Nel, W.; Sumner, P.D. Intensity, energy and erosivity attributes of rainstorms in the KwaZulu-Natal Drakensberg, South Africa. *S. Afr. J. Sci.* **2007**, *103*, 398–402.
50. UNEP. *World Atlas of Desertification*; Edward Arnold: London, UK, 1992.
51. McKee, T.B.; Doesken, N.J.; Kleist, J. The relationship of drought frequency and duration to time scales. In Proceedings of the 8th Conference on Applied Climatology, Anaheim, CA, USA, 17–22 January 1993; pp. 179–184.
52. Oliver, J.E. Monthly precipitation distribution: A comparative index. *Prof. Geogr.* **1980**, *32*, 300–309. [CrossRef]
53. Arnoldus, H.M.J. An approximation of the rainfall factor in the Universal Soil Loss Equation. In *Assessment of Erosion*; de Boodt, M., Gabriels, D., Eds.; FAO: Rome, Italy, 1980; pp. 127–132.
54. Tyson, P.D.; Lee-Thorp, J.; Holmgren, K.; Thackeray, J.F. Changing gradients of climate change in southern Africa during the past millennium: Implications for population movements. *Clim. Chang.* **2002**, *52*, 129–135. [CrossRef]
55. Membele, G.M.; Naidu, M.; Mutanga, O. Examining flood vulnerability mapping approaches in developing countries: A scoping review. *Int. J. Disaster Risk Reduct.* **2022**, *69*, 102766. [CrossRef]
56. Tfwala, C.M.; van Rensburg, L.D.; Schall, R.; Dlamini, P. Drought dynamics and interannual rainfall variability on the Ghaap plateau, South Africa, 1918–2014. *Phys. Chem. Earth* **2018**, *107*, 1–7. [CrossRef]
57. Roffe, S.J.; Steinkopf, J.; Fitchett, J.M. South African winter rainfall zone shifts: A comparison of seasonality metrics for Cape Town from 1841-1899 and 1933-2020. *Theoret. Appl. Climatol.* **2022**, *147*, 1229–1247. [CrossRef]
58. Ngobeni, D.; Knight, J. Evaluation of river mouth dynamics along the Eastern Cape coastline, South Africa. *Trans. R. Soc. S. Afr.* **2023**, *78*, 167–180. [CrossRef]
59. Kruger, A.C.; Nxumalo, M.P. Historical rainfall trends in South Africa: 1921–2015. *Water SA* **2017**, *43*, 285–297. [CrossRef]
60. Dyson, L.L.; van Heerden, J. The heavy rainfall and floods over the northeastern interior of South Africa during February 2000. *S. Afr. J Sci* **2001**, *97*, 80–86.
61. Liu, H.-Y.; Satoh, M.; Gu, J.-F.; Lei, L.; Tang, J.; Tan, Z.-M.; Wang, Y.; Xu, J. Predictability of the most long-lived tropical cyclone Freddy (2023) during its westward journey through the southern tropical Indian Ocean. *Geophys. Res. Lett.* **2023**, *50*, e2023GL105729. [CrossRef]
62. Kruger, A.C. The influence of the decadal-scale variability of summer rainfall on the impact of El Nino and La Nina events in South Africa. *Int. J. Climatol.* **1999**, *1*, 59–68. [CrossRef]
63. Meque, A.; Abiodun, B.J. Simulating the link between ENSO and summer drought in Southern Africa using regional climate models. *Clim. Dyn.* **2015**, *44*, 1881–1900. [CrossRef]
64. Diab, R.D.; Preston-Whyte, R.A.; Washington, R. Distribution of rainfall by synoptic type over Natal, South Africa. *Int. J. Climatol.* **1991**, *11*, 877–888. [CrossRef]
65. Mahlalela, P.T.; Blamey, R.C.; Reason, C.J.C. Mechanisms behind early winter rainfall variability in the southwestern Cape, South Africa. *Clim. Dyn.* **2019**, *53*, 21–39. [CrossRef]
66. MacKellar, N.; New, M.; Jack, C. Observed and modelled trends in rainfall and temperature for South Africa: 1960–2010. *S. Afr. J. Sci.* **2014**, *110*, 13. [CrossRef]
67. Weaver, A.vB. The distribution of soil erosion as a function of slope aspect and parent material in Ciskei, southern Africa. *GeoJournal* **1991**, *23*, 29–34. [CrossRef]
68. Le Roux, J.S.; Roos, Z.N. The effect of rainfall factors and antecedent soil moisture on soil loss on a low-angled slope in a semi-arid climate. *Water SA* **1991**, *17*, 179–182.
69. Kariaga, B.M. Rainfall erosivity factor for Uasin Gishu Plateau, Kenya. *Discov. Innov.* **2002**, *14*, 57–62.
70. Dunkerley, D. Rainfall intensity in geomorphology: Challenges and opportunities. *Prog. Phys. Geogr.* **2021**, *45*, 488–513. [CrossRef]
71. Wiggs, G.; Holmes, P. Dynamic controls on wind erosion and dust generation on west-central Free State agricultural land, South Africa. *Earth Surf. Process. Landf.* **2011**, *36*, 827–838. [CrossRef]
72. Grauso, S.; Diodato, N.; Verrubbi, V. Calibrating a rainfall erosivity assessment model at regional scale in Mediterranean area. *Environ. Earth Sci.* **2010**, *60*, 1597–1606. [CrossRef]
73. Salvador Sanchis, M.P.; Torri, D.; Borselli, L.; Poesen, J. Climate effects on soil erodibility. *Earth Surf. Proc. Landf.* **2008**, *33*, 1082–1097. [CrossRef]

74. de Vente, J.; Poesen, J.; Verstraeten, G.; Govers, G.; Vanmaercke, M.; Van Rompaey, A.; Arabkhedri, M.; Boix-Fayos, C. Predicting soil erosion and sediment yield at regional scales: Where do we stand? *Earth-Sci. Rev.* **2013**, *127*, 16–29. [CrossRef]
75. Dardis, G.F. Quaternary erosion and sedimentation in badland areas of southern Africa. *Catena Suppl.* **1989**, *14*, 1–9.
76. Dardis, G.F. Late Holocene erosion and colluvium deposition in Swaziland. *Geology* **1990**, *18*, 934–937. [CrossRef]
77. Shakesby, R.A.; Whitlow, R. Perspectives on Prehistoric and Recent Gullying in Central Zimbabwe. *GeoJournal* **1991**, *23*, 49–58. [CrossRef]
78. Seutloali, K.E.; Dube, T.; Mutanga, O. Assessing and mapping the severity of soil erosion using the 30-m Landsat multispectral satellite data in the former South African homelands of Transkei. *Phys. Chem. Earth* **2017**, *100*, 296–304. [CrossRef]
79. Keay-Bright, J.; Boardman, J. The influence of land management on soil erosion in the Sneeuberg Mountains, Central Karoo, South Africa. *Land Degrad. Develop.* **2007**, *18*, 423–439. [CrossRef]
80. Boardman, J.; Favis-Mortlock, D.; Foster, I. A 13-year record of erosion on badland sites in the Karoo, South Africa. *Earth Surf. Process Landf.* **2015**, *40*, 1964–1981. [CrossRef]
81. Benavidez, R.; Jackson, B.; Maxwell, D.; Norton, K. A review of the (Revised) Universal Soil Loss Equation ((R)USLE): With a view to increasing its global applicability and improving soil loss estimates. *Hydrol. Earth Syst. Sci.* **2018**, *22*, 6059–6086. [CrossRef]
82. Le Roux, J.J.; Newby, T.S.; Sumner, P.D. Monitoring soil erosion in South Africa at a regional scale: Review and recommendations. *S. Afr. J. Sci.* **2007**, *103*, 329–335.
83. Mararakanye, N.; Le Roux, J.J. Gully location mapping at a national scale for South Africa. *S. Afr. Geogr. J.* **2012**, *94*, 208–218. [CrossRef]
84. Knight, J. Stratigraphy and palaeoenvironmental interpretation of late Quaternary colluvial slope deposits in southern Africa. *S. Afr. J. Geol.* **2021**, *124*, 915–926. [CrossRef]
85. Ebhuoma, O.; Gebreslasie, M.; Ebhuoma, E.; Leonard, L.; Ngetar, N.S.; Zamisa, B. Farmers' perception of soil erosion and degradation and their effects on rural livelihoods in KwaMaye community, KwaZulu-Natal, South Africa. *J. Asian Afr. Stud.* **2023**, *58*, 1405–1421. [CrossRef]
86. Chapman, S.; Birch, C.E.; Galdos, M.V.; Pope, E.; Davie, J.; Bradshaw, C.; Eze, S.; Marsham, J.H. Assessing the impact of climate change on soil erosion in East Africa using a convection-permitting climate model. *Environ. Res. Lett.* **2021**, *16*, 084006. [CrossRef]
87. Claassen, D.; Botha, G.; Linol, B. An integrated assessment of erosion drivers facilitating gully expansion rates—A near century multi-temporal analysis from South Africa. *Land Degrad. Develop.* **2024**, *35*, 3675–3699. [CrossRef]

Disclaimer/Publisher's Note: The statements, opinions and data contained in all publications are solely those of the individual author(s) and contributor(s) and not of MDPI and/or the editor(s). MDPI and/or the editor(s) disclaim responsibility for any injury to people or property resulting from any ideas, methods, instructions or products referred to in the content.